Materials Chemistry and Physics 185 (2017) 210–217

Contents lists available at ScienceDirect

Materials Chemistry and Physics

journal homepage: www.elsevier.com/locate/matchemphys

Ab initio molecular dynamics study of lithium diffusion in tetragonal $Li_7La_3Zr_2O_{12}$

B. Andriyevsky [a, b, *], K. Doll [b, c], T. Jacob [b, d]

[a] Faculty of Electronics and Computer Sciences, Koszalin University of Technology, 2 Śniadeckich Str., PL-75-453, Koszalin, Poland
[b] Institute of Electrochemistry, Ulm University, Albert-Einstein-Allee 47, D-89069, Ulm, Germany
[c] Institute of Theoretical Chemistry, Pfaffenwaldring 55, D-70569, Stuttgart, Germany
[d] Helmholtz Institute Ulm (HIU) for Electrochemical Energy Storage[1], Albert-Einstein-Allee 11, D-89081, Ulm, Germany

HIGHLIGHTS

- Partial lithium atoms subtraction from LLZO increases diffusion coefficient $D^{(Li)}$.
- Partial subtraction of lithium atoms from LLZO decreases activation energy $E_a^{(Li)}$.
- Activation energy $E_a^{(Li)}$ is the smallest for tetrahedral oxygen surrounding.
- Compression of LLZO leads to a decrease of lithium ion diffusion coefficient $D^{(Li)}$.

ARTICLE INFO

Article history:
Received 14 May 2016
Received in revised form
22 September 2016
Accepted 16 October 2016
Available online 19 October 2016

Keywords:
Inorganic compounds
ab initio calculations
Molecular dynamics
Diffusion
Transport properties

ABSTRACT

Using *ab initio* density functional theory the thermally-stimulated migration of lithium ions in the garnet-type material $Li_7La_3Zr_2O_{12}$ is investigated. The methods of *ab initio* molecular dynamics have been applied to calculate the lithium ion self-diffusion coefficient and the diffusion barriers as function of lithium ion concentration. The concentration of lithium in the initial $Li_7La_3Zr_2O_{12}$ crystal unit cell is varied from 53 to 59 atoms, where 56 lithium atoms represent the stoichiometric concentration. Almost monotonous dependencies of the main characteristics on the number of lithium atoms $N^{(Li)}$ have been found, except for a non-monotonous peculiarity of the stoichiometric compound ($N^{(Li)} = 56$). Finally, the influence of the unit cell volume change on lithium ion diffusion parameters as well as lithium ion hopping rates has been studied.

1. Introduction

Over the last 30 years, development and application of solid electrolytes possessing high ionic conductivity at room temperature and high chemical stabilities have been achieved [1]. Currently, there is great interest in the application of solid electrolytes for high-performance lithium batteries because of the high electrical, chemical, and mechanical stability [2]. Therefore, strong efforts are at present directed towards improving the power density for advanced lithium batteries. Here mathematical modeling of solid-state batteries [3,4] has become an important tool to address the numerous phenomena at play during charge and discharge and to search for alternative or new materials with low activation energy for electric conductivity, *i.e.* low diffusion barriers between sites of light positive ions (*e.g.* Li^+, Na^+, Be^{2+}, Mg^{2+} ions).

Lithium-containing crystals of garnet-type structure are good candidates for battery electrolyte materials due to relatively low electronic conductivities and high electrochemical stabilities [5]. Amongst this class of materials $Li_7La_3Zr_2O_{12}$ (LLZO) was studied both experimentally and theoretically [6–17]. It was found that the lithium ion conductivity of the tetragonal structural modification of LLZO, $2 \cdot 10^{-6}$ S cm^{-1}, is comparable to that of the large group of structurally complex garnet-type compounds [18–25]. The lithium ion conductivity of LLZO with cubic symmetry is around two orders of magnitude higher and the corresponding

* Corresponding author. Faculty of Electronics and Computer Sciences, Koszalin University of Technology, Śniadeckich Str. 2, PL-75-453, Koszalin, Poland. Tel.: +48 94 3478 690; fax: +48 94 3433479.
E-mail address: bohdan.andriyevskyy@tu.koszalin.pl (B. Andriyevsky).
[1] Karlsruhe Institute of Technology (KIT), P.O. box 3640, 76021 Karlsruhe, Germany.

http://dx.doi.org/10.1016/j.matchemphys.2016.10.025
0254-0584/

activation energy for lithium diffusion is essentially smaller (0.34 eV in Al-stabilized cubic LLZO vs. 0.49 eV in Al-free tetragonal LLZO) [9]. However, the cubic modification of LLZO is structurally unstable, which limits its practical application in battery systems. Similar results had been reported in Ref. [7], with an activation energy of 0.54 eV in tetragonal LLZO and 0.3 eV in cubic LLZO [6]. An activation energy of about 0.5 eV for tetragonal LLZO was deduced in NMR experiments [26]. In classical molecular dynamics simulations, an initial barrier of 0.6 eV was observed for the tetragonal phase, which became 0.48 eV at high temperatures, and 0.34 eV when cooling down to low temperatures. The latter low barrier was explained due to remaining disorder [27]. Employing *ab initio* molecular dynamics simulations, a concerted mechanism with a barrier of 0.33 eV was suggested for cubic LLZO [10]. Further, from *ab-initio* molecular dynamics simulations, metadynamics and nudged elastic band calculations, two different mechanisms were identified: in the tetragonal phase, a synchronous mechanism with an activation energy of about 0.4 eV was observed; in the cubic phase, an asynchronous mechanism with a barrier of 0.1–0.3 eV.

In the present study we focus on the tetragonal modification of LLZO, whose crystalline unit cell ($a = b = 1.31$ nm and $c = 1.27$ nm) of the space group symmetry $I4_1/acd$ (no. 142) contains 8 formula units of $Li_7La_3Zr_2O_{12}$ and 56 lithium atoms at three different crystallographic sites: 8 atoms at the tetrahedral site $Li^{(1)}$ (four nearest neighbor distances to oxygen atoms are equal to 1.89 Å, 1.89 Å, 1.89 Å, and 1.89 Å, see Fig. 1a), 16 atoms at the octahedral site $Li^{(2)}$ (six nearest neighbor distances to oxygen atoms are equal to 1.93 Å, 1.93 Å, 2.34 Å, 2.34 Å, 2.44 Å, and 2.44 Å, see Fig. 1b) and 32 atoms at the less symmetrical tetrahedral site $Li^{(3)}$ (four nearest neighbor distances to oxygen atoms are equal to 1.85 Å, 2.02 Å, 2.04 Å, and 2.17 Å, see Fig. 1c) [7].

Performing *ab initio* DFT simulations we investigated the influence of these three different types of Li-atoms on the diffusion properties (partial diffusion coefficients and activation energies) as function of temperature and the overall lithium concentration [9,16,26]. One of the main goals was also the study of the impact of the lithium atom content of the tetragonal LLZO, ranging from 53 to 59 atoms in a crystal unit cell, on the characteristics of lithium ion self-diffusion.

1.1. Computational details

The *ab initio* molecular dynamics simulations of LLZO have been performed in the framework of density functional theory (DFT) using the VASP package [28]. The projector augmented-wave (PAW) method with a cutoff energy of 400 eV for the plane waves was employed [28,29], together with the corresponding pseudopotentials. For the exchange and correlation terms, the gradient corrected Perdew-Burke-Ernzerhof (PBE) functional was used. Taking the large unit cell of LLZO into account ($V_c = 2133$ Å^3) a k-point grid with 8 irreducible points was used for k-space summations.

The *ab initio* molecular dynamics (AIMD) calculations of LLZO were performed at the micro-canonical ensemble (NVE) for different temperatures at the unit cell volume corresponding to the initially optimized unit cell parameters at $T = 0$ K. For comparison, the AIMD calculations have also been performed with unit cell volumes corresponding to the thermally expanded material. Most results of AIMD calculations have been obtained for the simulation time up to 10 ps with the time step of 1 fs. For postprocessing analyses the post AIMD calculation program used was nMoldyn 3.0 [30].

Using the obtained AIMD-trajectories the mean-square displacements (MSD) were calculated by the following relation:

$$\sigma(t) = \frac{1}{N}\sum_{\alpha=1}^{N} w_\alpha \left\langle d_\alpha^2(t) \right\rangle \tag{1}$$

where, $\langle d_\alpha^2(t)\rangle$ denotes the MSD for ions of the α-type, $d_\alpha(t) = R_\alpha(t) - R_\alpha(0)$, w_α is the weight coefficient and t the time. Then the corresponding diffusion coefficient $D_\sigma^{(\alpha)}$ was obtained as

$$D_\sigma^{(\alpha)} = \lim_{t\to\infty} \frac{1}{6t}\sigma^{(\alpha)}(t) \tag{2}$$

Alternatively, we also used the velocity autocorrelation functions (VACF) to calculate the diffusion coefficients based on:

$$C_{vv}(t) = \frac{1}{3N}\sum_{\alpha=1}^{N} w_\alpha \langle v_\alpha(0)\cdot v_\alpha(t)\rangle \tag{3}$$

and its Fourier transform,

$$G(\omega) = \int_0^\infty \exp[-i\omega t] C_{vv}(t)dt \tag{4}$$

which is the spectral density of states (SDOS) $G(\omega)$. According to eq. (4) the value of SDOS at $\omega = 0$ gives the diffusion coefficient [30]:

$$D_G = \int_0^\infty C_{vv}(t)dt = G(0) \tag{5}$$

The experimental lithium ion specific conductivity (σ_{dc}) of tetragonal LLZO is of the order of 10^{-6} S cm^{-1} at ambient temperatures [7]. Taking into account the Nernst–Einstein relation [31],

$$D_\sigma = \frac{\sigma_{dc} k_B T}{nq^2} \tag{6}$$

and the corresponding values of n ($2.5\cdot10^{28}$ m^{-3}) and q ($1.6\cdot10^{-19}$ C) the diffusion coefficient of LLZO at $T = 300$ K is estimated to be around $D_\sigma = 0.64\cdot10^{-15}$ m^2/s $= 0.64\cdot10^{-9}$ nm^2/ps. Due to this relatively small D_σ value, the duration of AIMD simulations of 10 ps would not be sufficient to expect the ion diffusion migration distances comparable with the corresponding standard deviation (SD) at ambient temperatures. Therefore, our AIMD simulations were performed at more elevated temperatures at which the change of lithium ion MSD for 10 ps will be larger than the corresponding SD values.

To compare the AIMD results for the activation energy for lithium ion diffusion, we have calculated this value also using the nudged elastic band method (NEB) implemented in VASP [32].

2. Results and discussion

The calculations on the diffusion coefficient $D^{(Li)}$ of lithium ions in the tetragonal LLZO using relation (5) showed an Arrhenius type behavior:

$$D^{(Li)} = D_0 \exp\left(-\frac{E_a}{kT}\right) \tag{7}$$

where D_0 is a prefactor and E_a denotes the corresponding activation energy. For tetragonal LLZO the linear dependency $\ln(D_G^{(Li)}/$ nm^{2}ps^{-1}) versus $10^3/(T/K)$ leads to an activation energy of $E_a^{(Li)} = 0.36$ eV (Fig. 2). That is comparable with the experimental magnitude [6,7,9].

Similar AIMD simulations have been performed for LLZO with a

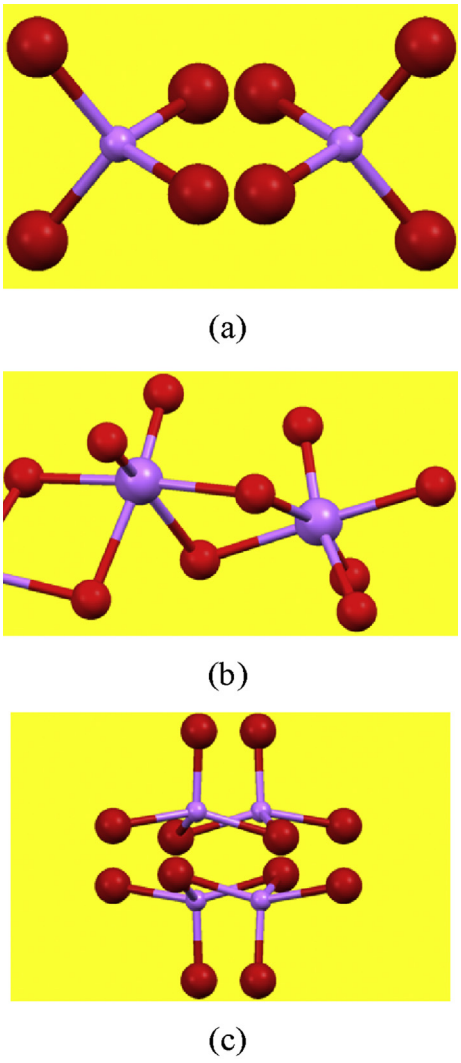

Fig. 1. Characteristic fragments of atomic structures of tetragonal LLZO with lithium (purple) and nearest neighbor oxygen (red) atoms of (a) lithium at $Li^{(1)}$ site, (b) lithium at $Li^{(2)}$ site, and (c) lithium at $Li^{(3)}$ site. For more clarity, the interatomic distances larger than 2.5 Å are not shown by sticks. (For interpretation of the references to colour in this figure legend, the reader is referred to the web version of this article.)

deficiency or excess of 1, 2, and 3 lithium atoms (based on 56 lithium atoms per unit cell for stoichiometric LLZO). For this purpose, successively one lithium atom on site 3 ($N_{Li} = 55$), another on site 2 ($N_{Li} = 54$), and another on site 1 ($N_{Li} = 53$) were removed. The structures obtained were structurally optimized and used for the subsequent AIMD calculations. Similarly, for the systems with higher lithium contents, additional lithium atoms (1, 2 or 3 for $N_{Li} = 57$, $N_{Li} = 58$, $N_{Li} = 59$) were inserted between two lithium atoms of site 3, and subsequently optimized. The corresponding results of the dependency $\ln(D_G^{(Li)}/nm^2ps^{-1})$ vs. $10^3T^{-1}/K^{-1}$ for these Li concentrations are shown in Fig. 3. These results relate to the temperature range $T > 1150$ K. For constant temperatures, the largest self-diffusion coefficients were obtained for concentrations of 53 and 54 lithium ions per unit cell (Fig. 3). It is also remarkable that for stoichiometric LLZO (*i.e.* 56 Li) the self-diffusion coefficient D_G is one of the smallest overall. This is similar to the situation of an undoped semiconductor. When an additional Li atom is inserted or removed, this would be similar to doping a semiconductor with electrons or removing them, and thus increasing the conductivity. In other words, a deviation of the lithium atom number from the

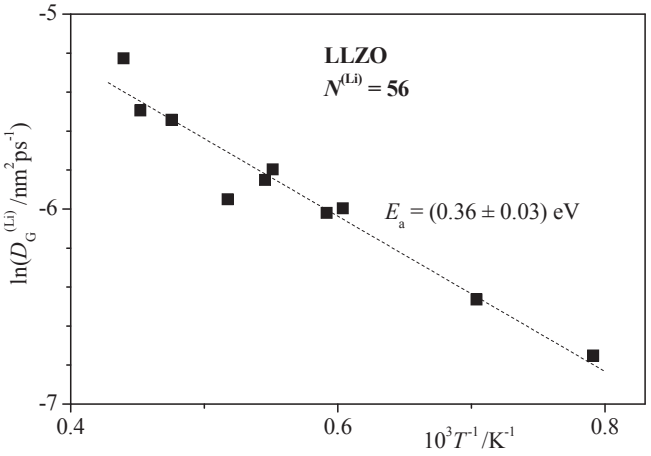

Fig. 2. Dependency of the logarithm of the diffusion coefficient on the inverse temperature for lithium ions in stoichiometric ($N^{(Li)} = 56$) tetragonal LLZO. The dashed straight line is a linear fit of the points. The value $E_a = 0.36$ eV is an activation energy of lithium ion self diffusion. The relative errors of the corresponding intercepts and slopes are the following: $\Delta(\ln(D_G^{(Li)}))/\ln(D_G^{(Li)}) = 0.05$, $\Delta E_a/E_a = 0.08$.

stoichiometric content (56 atoms) should lead unambiguously to the increase of the local crystal structure distortion and consequently to the corresponding decrease of binding energy and increase of diffusion coefficient of the neighboring lithium ions. The absolute value of the slope of the linear dependency of $\ln(D_G^{(Li)}/nm^2ps^{-1})$ vs. $10^3T^{-1}/K^{-1}$ is proportional to the activation energy E_a (Eq. (7)). Results of the corresponding fittings are presented in Fig. 4. Overall there seems to be a linear increase of E_a with the number of lithium atoms $N^{(Li)}$. Further, there is an additional raise around the stoichiometric content of LLZO ($N^{(Li)} = 56$). This is due to the relatively high stability of stoichiometric LLZO where all high symmetry sites are filled, and no vacancies or interstitials exist.

At fixed temperature, the diffusion coefficient D_G of LLZO as function of the lithium ion number $N^{(Li)}$ in the crystalline unit cell (derived from the data of Fig. 3) shows generally a decreasing dependency (Fig. 5). Increasing the number of lithium atoms from 53

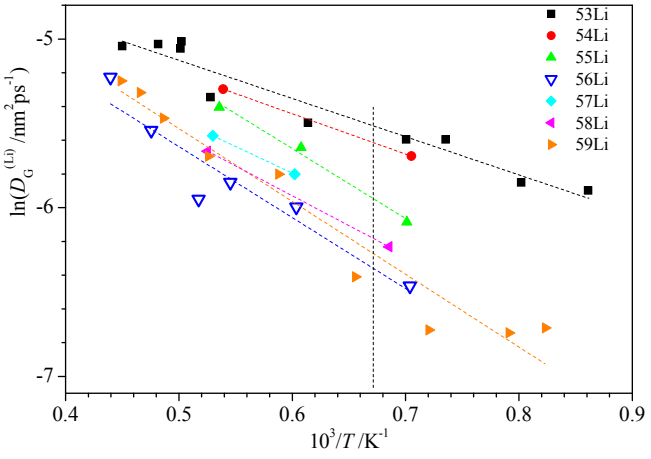

Fig. 3. Logarithm of the diffusion coefficient as function of the inverse temperature for different number of lithium ions in the crystalline LLZO unit cell. The inclined dashed straight lines indicate the linear fit of the corresponding points. The relative errors of the corresponding intercepts $\Delta(\ln(D_G))/\ln(D_G)$ and slopes $\Delta E_a/E_a$ are the following: $\Delta(\ln(D_G^{(53Li)}))/\ln(D_G^{(53Li)}) = 0.03$, $\Delta E_a^{(53Li)}/E_a^{(53Li)} = 0.09$; $\Delta(\ln(D_G^{(55Li)}))/\ln(D_G^{(55Li)}) = 0.08$, $\Delta E_a^{(55Li)}/E_a^{(55Li)} = 0.10$; $\Delta(\ln(D_G^{(56Li)}))/\ln(D_G^{(56Li)}) = 0.11$, $\Delta E_a^{(56Li)}/E_a^{(56Li)} = 0.17$; $\Delta(\ln(D_G^{(59Li)}))/\ln(D_G^{(59Li)}) = 0.07$, $\Delta E_a^{(59Li)}/E_a^{(59Li)} = 0.09$. The vertical dashed line marks the temperature $T = 1500$ K.

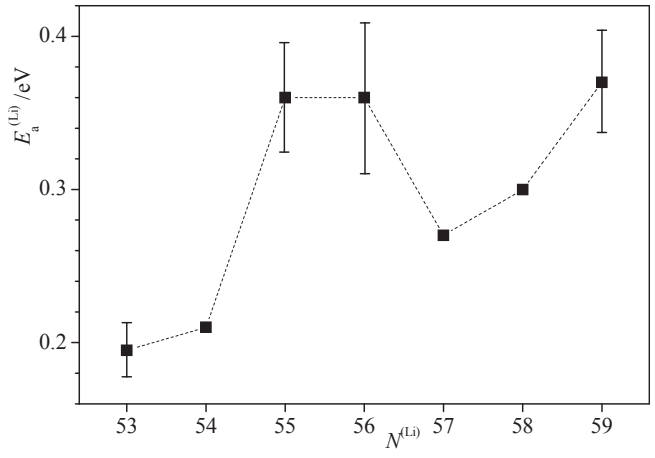

Fig. 4. Dependency of the activation energy $E_a^{(Li)}$ on the number of lithium ions $N^{(Li)}$ in the LLZO unit cell (derived from Fig. 3).

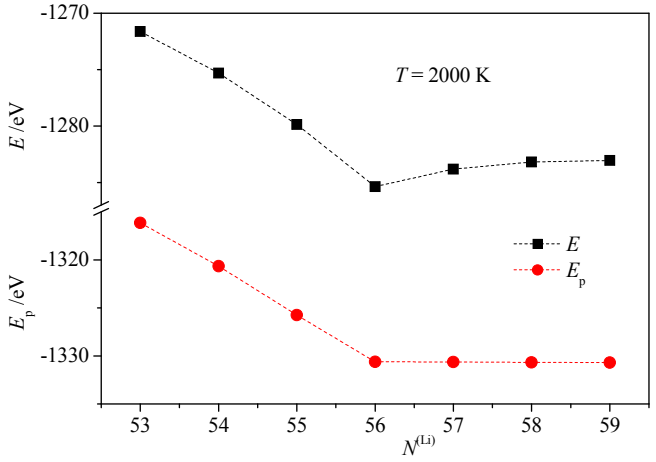

Fig. 6. Dependencies of the averaged total (E) and potential (E_p) energies on the number of lithium ions $N^{(Li)}$ in the unit cell of LLZO for the fixed temperature $T = 2000$ K.

to 59 halves the diffusion coefficient $D_G^{(Li)}$. The local minimum of D_G at $N^{(Li)} = 56$ (Fig. 5) may be explained by the fact that this stoichiometric content of LLZO is the most relatively stable one, among the lithium concentrations considered in the present work. A deviation of the lithium atom number from the stoichiometric content (56 atoms) should lead unambiguously to the increase of the local crystal structure distortion and consequently to the corresponding decrease of binding energy and increase of diffusion coefficient of the neighboring lithium ions. This suggestion is supported by the dependencies of the averaged total and potential energies on the number of lithium atoms in the crystal unit cell of LLZO (Fig. 6).

As tetrahedral LLZO contains three symmetry-different lithium sites in the crystalline unit cell (denoted as $Li^{(1)}$, $Li^{(2)}$, and $Li^{(3)}$) [7], we have studied using AIMD, the dependencies of $\ln(D_G^{(Li)}/nm^2ps^{-1})$ vs. $10^3T^{-1}/K^{-1}$ (comparable to Fig. 3) and have obtained the activation energy E_a for these different sites separately. The corresponding results are summarized in Table 1.

The activation energies $E_a^{(1)}$, $E_a^{(2)}$, and $E_a^{(3)}$ for the sites $Li^{(1)}$, $Li^{(2)}$, and $Li^{(3)}$ and the averaged $E_a^{(av)}$ value for all lithium ions were found to be clearly different (Table 1), that indicates the influence of the lithium site symmetry on the activation energy E_a. For three lithium contents ($N_{Li} = 53$, 56, and 59) we find the relations $E_a^{(1)} \approx E_a^{(3)} < E_a^{(2)}$. The smallest averaged activation energy $E_a^{(av)} = 0.19$ eV is obtained for the lowest Li concentration ($N = 53$). It is interesting that for LLZO with $N^{(Li)} = 53$, the activation energies $E_a^{(1)}$, $E_a^{(2)}$, and $E_a^{(3)}$ for three different lithium sites are similar, leading to a similar averaged value of $E_a^{(av)} = 0.19$ eV. This low $E_a^{(av)}$ value can be explained due to the large number of vacant lithium sites, which in fact facilitate the increase of the local electric field from the nearest negative oxygen ions thus decreasing the energy barriers for the lithium ion migration. Similarly, increase of the additional lithium atoms in LLZO ($N^{(Li)} > 56$) should limit the probability of the lithium ion migration, that is manifested in the corresponding increase of the energy barriers and decrease of the diffusion coefficient for the lithium ion migration (see Figs. 4 and 5 and Table 1). For stoichiometric LLZO ($N^{(Li)} = 56$), diffusion through the faces of the tetrahedra built of the oxygen atoms surrounding the lithium atoms $Li^{(1)}$ or $Li^{(3)}$ is found to be easier than in the case of $Li^{(2)}$ with diffusion through the faces of an octahedron.

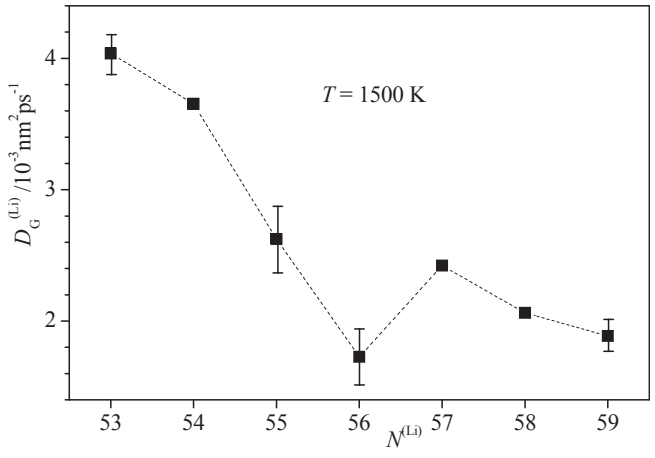

Fig. 5. Dependency of the lithium ion diffusion coefficient $D_G^{(Li)}$ on the number of ions $N^{(Li)}$ in the unit cell of LLZO for the fixed temperature $T = 1500$ K.

In this context, the molecular dynamics study of alkali metal vapors [33] and of ionic compounds [34] is interesting. In the case of ionic compounds such as NaCl and KCl, it was observed that not only neutral ion pairs, quartets and sextets, but also charged clusters play an important role. At high temperature, diffusion coefficients were observed to be in inverse proportion to the ionic mass.

In view of relationship (5) between the diffusion coefficient D_G and the spectral density of states $G(0)$ we have studied changes in the frequency dependency $G(f)$, with $f = \omega/2\pi$, as function of the lithium content. The results are summarized in Figs. 7–9 for LLZO lithium contents of $N^{(Li)} = 53$, 56, and 59. The SDOS frequency distributions $G(f)$ for the three different lithium sites $Li^{(1)}$, $Li^{(2)}$, and $Li^{(3)}$ all show one main maximum, which shifts with lithium content. For $Li^{(1)}$ sites the maxima are shifted to higher frequencies in

Table 1
The activation energy E_a of the tetragonal LLZO obtained for different lithium ion numbers $N^{(Li)}$ in the crystal unit cell and different lithium ion sites $Li^{(1)}$, $Li^{(2)}$, and $Li^{(3)}$ at the temperature range $T > 1350$ K by using AIMD. The uncertainty $\Delta E_a/E_a \approx 0.1$.

Activation energy E_a/eV	Number of lithium ions $N^{(Li)}$		
	53	56	59
$E_a^{(1)}$	0.20	0.31	0.50
$E_a^{(2)}$	0.21	0.43	0.50
$E_a^{(3)}$	0.19	0.35	0.44
$E_a^{(av)}$	0.19	0.36	0.46

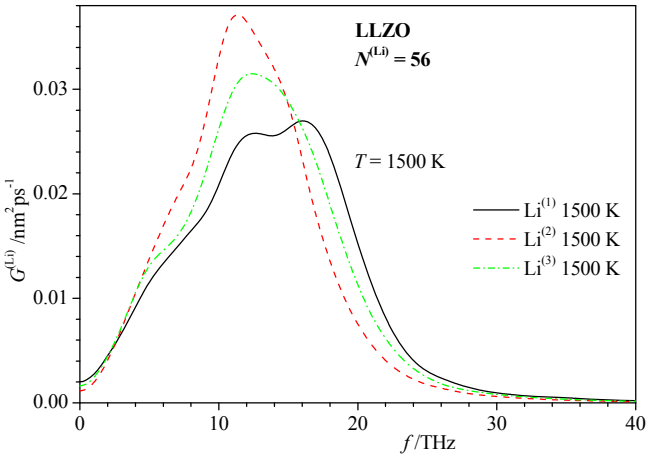

Fig. 7. SDOS $G^{(Li)}$ vs. frequency f of stoichiometric LLZO with 56 lithium atoms convoluted for the three different lithium sites $Li^{(1)}$, $Li^{(2)}$, and $Li^{(3)}$ at $T = 1500$ K.

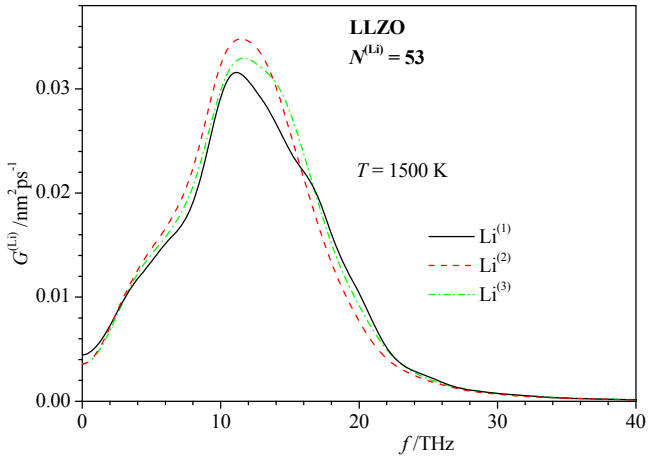

Fig. 9. SDOS $G^{(Li)}$ vs. frequency f of LLZO with 53 lithium atoms convoluted for the three different lithium sites $Li^{(1)}$, $Li^{(2)}$, and $Li^{(3)}$ (three lithium vacancies at $Li^{(1)}$, $Li^{(2)}$, and $Li^{(3)}$) at $T = 1500$ K.

contrast to the SDOS maxima for $Li^{(3)}$ and $Li^{(2)}$ sites, showing the opposite behavior. Comparing the three different systems we always find lower frequency values for $Li^{(2)}$ sites compared to $Li^{(1)}$ and $Li^{(3)}$ sites. Moreover, a clear correlation is observed between the SDOS of the three sites $Li^{(1)}$, $Li^{(2)}$, $Li^{(3)}$ and the main characteristics of the lithium ions self diffusion – the diffusion coefficient D_G (Fig. 5) and the activation energy E_a (Fig. 4): the more similar the SDOS and thus the more similar the frequency spectrum for the three sites, the smaller the activation energy E_a and the larger the diffusion coefficient D_G. This correlation may be caused by the resonance phenomena taking place in the ensemble of the thermally vibrating lithium ions.

Another feature of the frequency SDOS distributions is that the highest value of $G(0) = D_G$ is observed for the lithium sites $Li^{(1)}$, for which the largest width of the distribution is observed in the whole range from 0 to 40 THz (Figs. 7–9). This feature may be an evidence for a large anharmonicity in the thermal vibrations of the effective lithium ion at site $Li^{(1)}$. Consequently, the fractional part of the low-frequency harmonic components of the lithium ion thermal vibrations at sites $Li^{(1)}$ is largest in comparison to the two other sites $Li^{(2)}$ and $Li^{(3)}$. According to relations (4) and (5), the zero frequency limit of these low-frequency components of SDOS $G(f \rightarrow 0)$ should be equal to the diffusion coefficient D_G.

We have also studied the influence of thermal expansion of tetragonal LLZO on the characteristics of lithium ion diffusion using the mean coefficient of the thermal linear expansion $\alpha_T = 2 \cdot 10^{-5}$ K^{-1} [17]. By comparing two different unit cell volumes $V_{c0} = 2133$ Å^3 (non-expanded) and $V_{cT} = 2331$ Å^3 (thermally expanded) at $T = 1500$ K we find that thermal expansion leads to an increase of the diffusion coefficient: $D_G^{(Li)}(V_{c0}) = 0.00184$ nm^{2}ps^{-1} and $D_G^{(Li)}(V_{cT}) = 0.0037$ nm^{2}ps^{-1} (Figs. 10 and 11). Simultaneously, the activation energy for lithium diffusion at $T = 1500$ K changes only marginally from $E_a^{(Li)}(V_{c0}) = 0.36$ eV in non-expanded LLZO to $E_a^{(Li)}(V_{cT}) = 0.38$ eV in the thermally-expanded structure (Fig. 10). The main difference is the prefactor D_0. Further, there is a clear low-frequency shift of the SDOS distribution together with an increase of the $\sigma(t)$ slope when expanding the LLZO unit cell (Fig. 11). This frequency shift is related to an increase of the amplitude and anharmonicity of lithium thermal vibrations, finally facilitating bond breaking and migration events in the material. Further, this leads to an overall increase of the diffusion coefficient (Figs. 10 and 11).

For comparison, also NEB calculations were performed. The NEB-path corresponds to the concerted lithium movement in the

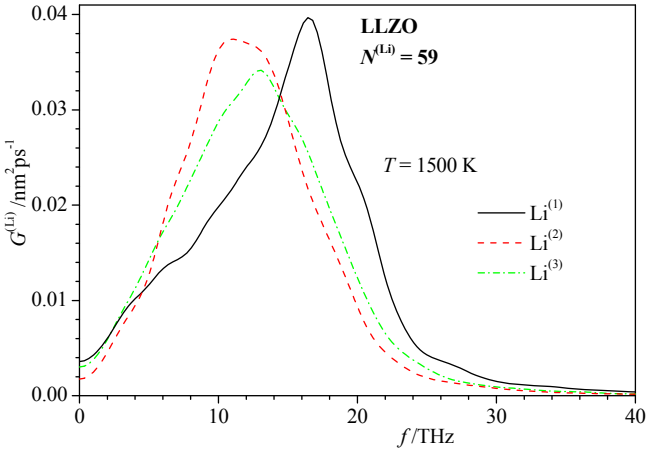

Fig. 8. SDOS $G^{(Li)}$ vs. frequency f of LLZO with 59 lithium atoms convoluted for the three different lithium sites $Li^{(1)}$, $Li^{(2)}$, and $Li^{(3)}$ at $T = 1500$ K.

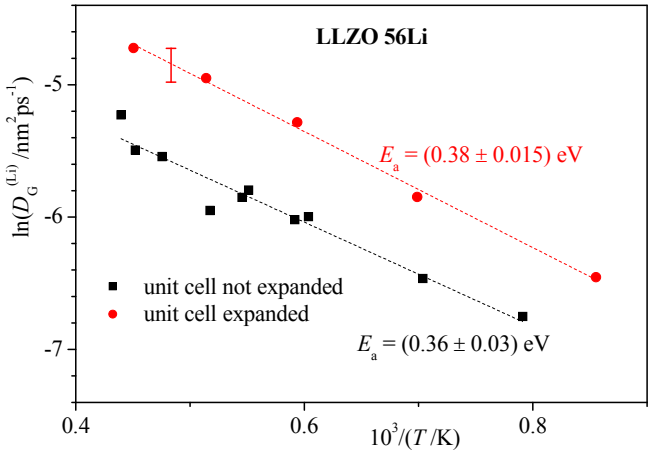

Fig. 10. Logarithm of the diffusion coefficient as function of the inverse temperature for 56 lithium ions in the optimized LLZO at $T = 0$ K (squares, unit cell volume $V = 2.133$ nm^3) and thermally expanded structure at $T = 1500$ K (circles, unit cell volume $V = 2.331$ nm^3). The inclined dashed straight lines indicate the linear fit of the corresponding points. The relative errors of the corresponding intercepts and slopes are the following: $\Delta(\ln(D_G^{(nonexp)}))/\ln(D_G^{(nonexp)}) = 0.11$, $\Delta E_a^{(nonexp)}/E_a^{(nonexp)} = 0.17$; $\Delta(\ln(D_G^{(exp)}))/\ln(D_G^{(exp)}) = 0.04$, $\Delta E_a^{(exp)}/E_a^{(exp)} = 0.04$.

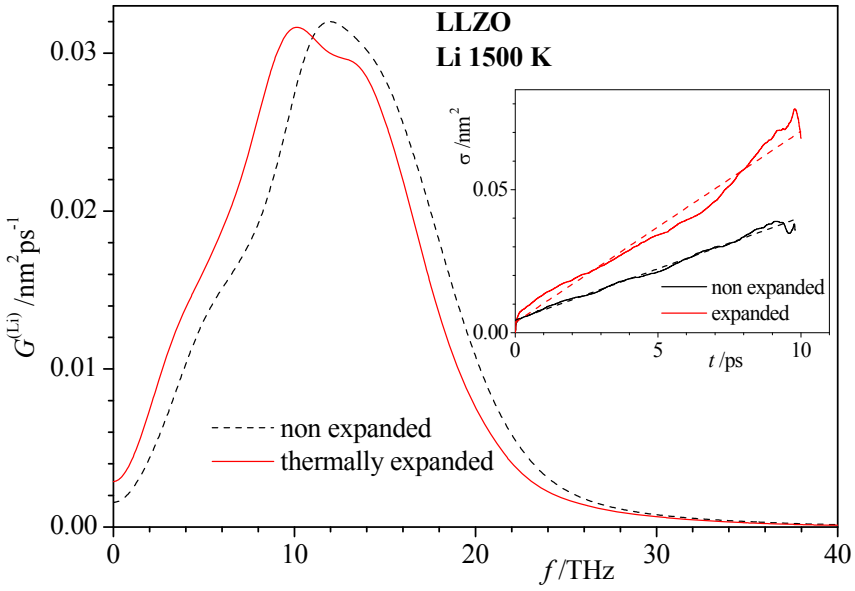

Fig. 11. SDOS $G^{(Li)}$ as function of the frequency f for 56 lithium ions in the non-expanded (dash) and thermally-expanded (solid) unit cell of LLZO. The inset shows the corresponding time dependencies of MSD $\sigma(t)$.

stoichiometric LLZO with 56 lithium atoms [14], where the activation energy E_a was found to be in the range of 0.41 eV–0.44 eV. In the present NEB calculations for the stoichiometric *LLZO*, performed in the same concerted way as in Ref. [14], we obtain the activation energy $E_a = E_{12} = 0.39$ eV (Fig. 12), which compares well with the similar value from Ref. [14]. The NEB barrier is thus sligthly larger than the activation energy $E_a = 0.36$ eV of lithium ion diffusion in non-expanded tetragonal LLZO obtained from AIMD simulations (Fig. 10 and Table 1).

The results of the present AIMD study are in good agreement with corresponding experimental studies of tetragonal LLZO performing diffusion-induced lithium spin-lattice relaxation NMR spectroscopy [26], and impedance spectroscopy [7] (Fig. 13). In Fig. 13, the jump rate τ^{-1} of lithium ions is calculated from the relation

$$DG = \left(a^2/6\right)\tau^{-1} \tag{8}$$

where D_G is the diffusion coefficient and $a = 0.2$ nm is taken as the averaged Li–Li jump distance in LLZO [26]. AIMD results on the temperature dependency of τ^{-1} for thermally expanded LLZO show a clear correspondence to the experimental data (Fig. 13). The calculated pre-exponential factor (frequency) τ_0^{-1} of the relation

$$\tau^{-1} = \tau_0^{-1} \exp(-E_a/k_B T) \tag{9}$$

for the case of the thermally expanded LLZO is found to be $\tau_0^{-1} = 10$ THz, that corresponds to the wavenumber $\nu = 333.6$ cm^{-1}. It is remarkable that the value $\tau_0^{-1} = 10$ THz is close to the center of the SDOS frequency distribution for LLZO (Figs. 7–9 and 11).

The time dependencies of MSD $\sigma(t)$ obtained for various ions of LLZO indicate no migrating ions at the ambient temperature $T = 300$ K and up to simulation temperatures of 981 K. However, at a simulation temperature of 1264 K, the lithium ions now show a linear increase of the MSD (Fig. 14), i.e. a real lithium ion diffusion

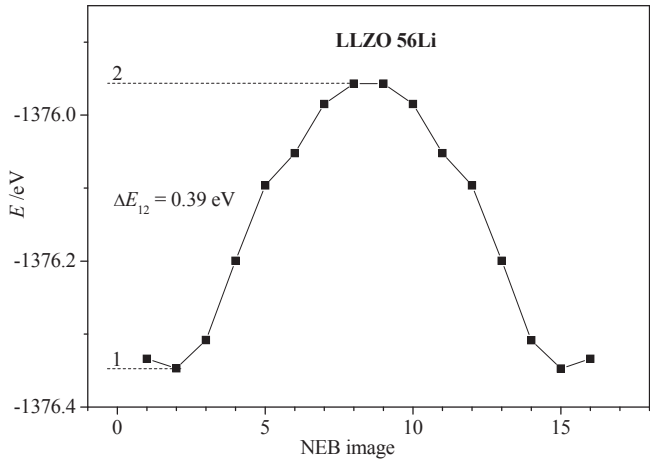

Fig. 12. Dependency of the minimum potential energy E on the NEB image for the concerted six-lithium ions migration pathway in tetragonal LLZO.

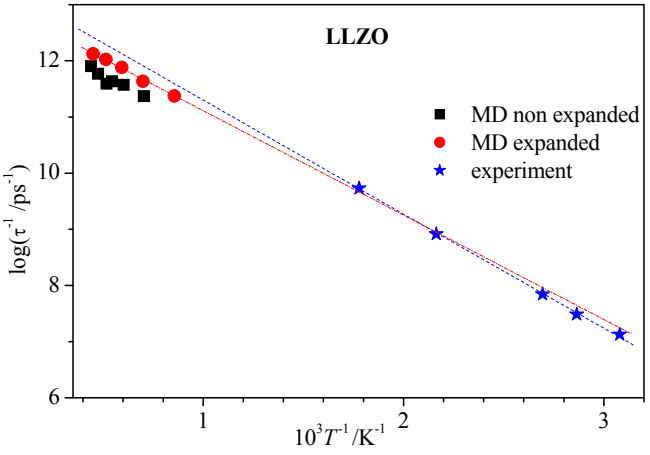

Fig. 13. Dependencies of the lithium ion jump rate for tetragonal LLZO on the inverse temperature obtained from AIMD simulations of the optimized structure at $T = 0$ K (squares, unit cell volume $V = 2.133$ nm^3) and the thermally expanded structure at $T = 1500$ K (circles, unit cell volume $V = 2.331$ nm^3). For comparison, the experimental data are shown as stars [7,26].

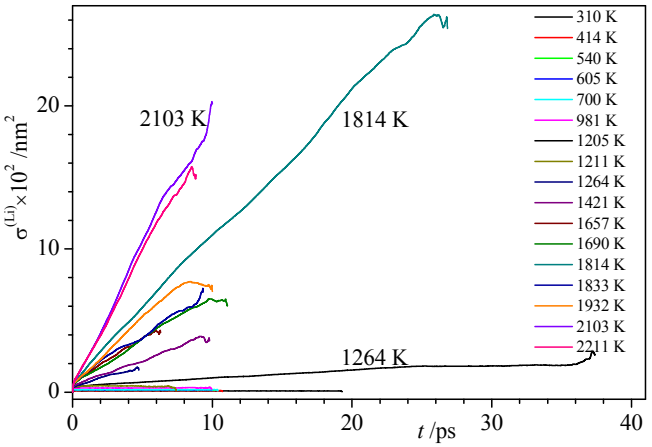

Fig. 14. Time dependencies of MSD $\sigma(t)$ of lithium ions of LLZO at different averaged temperatures.

takes place. The other ions (La, Zr, and O) do not show diffusion, as expected.

3. Conclusions

Using *ab initio* density functional theory the thermally-stimulated migration of lithium ions in the garnet-type material $Li_7La_3Zr_2O_{12}$ (LLZO) was investigated with varying lithium ion concentration (ranging from 53 to 59 atoms, where 56 lithium atoms represent the stoichiometric concentration). We find that:

1. The analysis of the AIMD results for tetragonal LLZO shows an observable migration at temperatures from 1250 K onwards, with the typical behavior of an MSD, which increases linearly with simulation time.
2. The activation energy $E_a^{(Li)}$ of lithium ion diffusion in tetragonal LLZO as function of lithium content $N^{(Li)}$ (between 53 and 59) increases gradually from 0.19 to 0.37 eV. The activation energy of stoichiometric LLZO ($N^{(Li)} = 56$) of $E_a^{(Li)} = 0.36$ eV deviates from this dependency towards higher $E_a^{(Li)}$ values, indicating that structural defects in LLZO lead to a decrease of $E_a^{(Li)}$. As a result, the diffusion coefficient $D^{(Li)}$ was found to be a decreasing function of the unit cell lithium content $N^{(Li)}$.
3. Three structurally different sites of lithium in tetragonal LLZO were distinguished, showing characteristically different activation energies in the order $E_a^{(Li1)} \approx E_a^{(Li3)} < E_a^{(Li2)}$. The activation energies $E_a^{(Li1)}$ and $E_a^{(Li3)}$ correspond to the tetrahedral and distorted tetrahedral oxygen nearest neighbor environments of lithium, while the energy $E_a^{(Li2)}$ corresponds to the distorted octahedral environment. The SDOS frequency dependencies for the various sites $Li^{(1)}$, $Li^{(2)}$, $Li^{(3)}$ are most similar for the smallest lithium content $N^{(Li)} = 53$, and less similar for the larger lithium content $N^{(Li)} = 56$ or 59. This is correlated with the smallest value of the activation energy $E_a^{(Li)} = 0.19$ eV, and is expected to be due to the influence of the resonance interactions between lithium ions.
4. One of the factors influencing the increase of the diffusion coefficient in LLZO is the degree of anharmonicity in lithium ion thermal vibrations: the larger the frequency width of the SDOS lithium ion distribution, the larger is the anharmonicity of the effective lithium ion vibration and the larger is the corresponding diffusion coefficient.
5. The unit cell volume compression of LLZO (about 10%) essentially leads to a decreasing lithium diffusion coefficient D (about 50%), mainly due to a reduced constant D_0 in the corresponding Arrhenius equation. At the same time the corresponding activation energy E_a decreases by only about 5%.

Acknowledgements

The authors gratefully acknowledge support from the German Academic Exchange Service (DAAD) under the research project "*First principles study of lithium ion migration in the garnet type crystals*" (Referat: 323, Kennziffer: A/14/05573, Haushaltstitel: 331 4 03 151). Calculations were performed partly in the computer centers ICM of Warsaw University (the project G26-3) and WCSS of Wrocław Technical University. Finally, TJ acknowledges support from the DFG (Deutsche Forschungsgemeinschaft) and the European Research Council through the ERC-Starting Grant THEOFUN (Grant Agreement No. 259608).

References

[1] T. Kudo, K. Fueki, Solid State Ionics, Wiley-VCH Verlag GmbH, Weinheim., Germany, 1990.
[2] B.B. Owens, in: B. Scrosati (Ed.), Fast Ion Transport in Solids, Kluwer Academic Press, Dordrecht, 1993.
[3] M. Landstorfer, S. Funken, T. Jacob, An advanced model framework for solid electrolyte intercalation batteries, Phys. Chem. Chem. Phys. 13 (2011) 12817–12825.
[4] M. Landstorfer, T. Jacob, Mathematical modeling of intercalation batteries at the cell level and beyond, Chem. Soc. Rev. 42 (2013) 3234–3252.
[5] V. Thangadurai, W. Weppner, $Li_6ALa_2Nb_2O_{12}$ (A = Ca, Sr, Ba): a new class of fast lithium ion conductors with garnet-like structure, J. Am. Ceram. Soc. 88 (2005) 411–418.
[6] R. Murugan, V. Thangadurai, W. Weppner, Fast lithium ion conduction in garnet-type $Li_7La_3Zr_2O_{12}$, Angew. Chem. Int. Ed. 46 (2007) 7778–7781.
[7] J. Awaka, N. Kijima, H. Hayakawa, J. Akimoto, Synthesis and structure analysis of tetragonal Li7La3Zr2O12 with the garnet-related type structure, J. Solid State Chem. 182 (2009) 2046–2052.
[8] E.J. Cussen, Structure and ionic conductivity in lithium garnets, J. Mater. Chem. 20 (2010) 5167–5173.
[9] H. Buschmann, J. Doelle, S. Berendts, A. Kuhn, P. Bottke, M. Wilkening, P. Heitjans, A. Senyshyn, H. Ehrenberg, A. Lotnyk, V. Duppel, L. Kienle, J. Janek, Structure and dynamics of the fast lithium ion conductor $Li_7La_3Zr_2O_{12}$, Phys. Chem. Chem. Phys. 13 (2011) 19378–19392.
[10] R. Jalem, Y. Yamamoto, H. Shiiba, M. Nakayama, H. Munakata, T. Kasuga, K. Kanamura, Concerted migration mechanism in the Li ion dynamics of garnet-type $Li_7La_3Zr_2O_{12}$, Chem. Mater 25 (2013) 425–430.
[11] M. Xu, M.S. Park, J.M. Lee, T.Y. Kim, Y.S. Park, E. Ma, Mechanisms of Li+ transport in garnet-type cubic Li3+xLa3M2O12 (M = Te, Nb, Zr), Phys. Rev. B 85 (2012) 052301–052305.
[12] N. Bernstein, M.D. Johannes, K. Hoang, Origin of the structural phase transition in $Li_7La_3Zr_2O_{12}$, Phys. Rev. Lett. 109 (2012) 205702–205705.
[13] G. Larraz, A. Orera, M.L. Sanjuan, Cubic phases of garnet-type Li7La3Zr2O12: the role of hydration, J. Mater. Chem. A 1 (2013) 11419–11428.
[14] K. Meier, T. Laino, A. Curioni, Solid-state electrolytes: revealing the mechanisms of Li-ion conduction in tetragonal and cubic LLZO by first-principles calculations, J. Phys. Chem. C 118 (2014) 6668–6679.
[15] J. Tan, A. Tiwari, Fabrication and characterization of $Li_7La_3Zr_2O_{12}$ thin films for lithium ion battery, ECS Solid State Lett. 1 (2012) Q57–Q60.
[16] W. Gu, M. Ezbiri, R. Prasada Rao, M. Avdeev, S. Adams, Effects of penta- and trivalent dopants on structure and conductivity of $Li_7La_3Zr_2O_{12}$, Solid State Ionics 274 (2015) 100–105.
[17] Y. Chen, E. Rangasamy, C.R. dela Cruz, C. Liang, Ke An, A study of suppressed formation of low-conductivity phases in doped $Li_7La_3Zr_2O_{12}$ garnets by in situ neutron diffraction, J. Mater. Chem. A 3 (2015) 22868–22876.
[18] V. Thangadurai, H. Kaack, W. Weppner, Novel fast lithium ion conduction in garnet-type $Li_5La_3M_2O_{12}$ (M = Nb, Ta), J. Am. Ceram. Soc. 86 (2003) 437–440.
[19] V. Thangadurai, S. Adams, W. Weppner, Crystal structure revision and identification of Li^+-ion migration pathways in the garnet-like $Li_5La_3M_2O_{12}$ (M = Nb, Ta) oxides, Chem. Mater 16 (2004) 2998–3006.
[20] V. Thangadurai, W. Weppner, $Li_6ALa_2Ta_2O_{12}$ (A = Sr, Ba): novel garnet-like oxides for fast lithium ion conduction, Adv. Funct. Mater 15 (2005) 107–112.
[21] V. Thangadurai, W. Weppner, Investigations on electrical conductivity and chemical compatibility between fast lithium ion conducting garnet-like Li6BaLa2Ta2O12 and lithium battery cathodes, J. Power Sources 142 (2005) 339–344.
[22] P. Knauth, J. Schoonman (Eds.), Nanocomposites—ionic Conducting Materials and Structural Spectroscopies, Springer, New York, 2007.
[23] R. Murugan, W. Weppner, P. Schmid-Beurmann, V. Thangadurai, Structure and lithium ion conductivity of garnet-like $Li_5La_3Sb_2O_{12}$ and $Li_6SrLa_2Sb_2O_{12}$, Mater. Res. Bull. 43 (2008) 2579–2591.

[24] A. Ramzy, V. Thangadurai, Tailor-made development of fast Li ion conducting garnet-like solid electrolytes, ACS Appl. Mater. Interfaces 2 (2010) 385–390.
[25] D. Rettenwander, P. Blaha, R. Laskowski, K. Schwarz, P. Bottke, M. Wilkening, C.A. Geiger, G. Amthauer, D. Rettenwander, P. Blaha, R. Laskowski, K. Schwarz, P. Bottke, M. Wilkening, C.A. Geiger, G. Amthauer, DFT study of the role of Al^{3+} in the fast ion-conductor $Li_{7-3x}Al^{3+}{}_xLa_3Zr_2O_{12}$ garnet, Chem. Mater 26 (2014) 2617–2623.
[26] A. Kuhn, S. Narayanan, L. Spencer, G. Goward, V. Thangadurai, M. Wilkening, Li self-diffusion in garnet-type Li7La3Zr2O12 as probed directly by diffusion-induced ^{7}Li spin-lattice relaxation NMR spectroscopy, Phys. Rev. B 83 (2011) 094302–094311.
[27] S. Adams, R.P. Rao, Ion transport and phase transition in Li7-x La3(Zr2-xMx) O12 (M = Ta5+, Nb5+, x=0, 0.25), J. Mat. Chem. 22 (2012) 1426–1434.
[28] G. Kresse, D. Joubert, From ultrasoft pseudopotentials to the projector augmented-wave method, Phys. Rev. B 59 (1999) 1758; G. Kresse, M. Marsman, J. Furthmüller, http://cms.mpi.univie.ac.at/vasp/vasp/vasp.html, Vienna, October, 2015.
[29] P.E. Blöchl, Projector augmented-wave method, Phys. Rev. B 50 (1994) 17953–17979.
[30] T. Róg, K. Murzyn, K. Hinsen, G.R. Kneller, nMoldyn: a program package for a neutron scattering oriented analysis of molecular dynamics simulations, J. Comput. Chem. 24 (2003) 657–667.
[31] P. Heitjans, S. Indris, Diffusion and ionic conduction in nanocrystalline ceramics, J. Phys. Condens. Matter 15 (2003) R1257–R1289.
[32] G. Mills, H. Jonsson, G.K. Schenter, Reversible work transition state theory: application to dissociative adsorption of hydrogen, Surf. Sci. 324 (1995) 305–337.
[33] V.V. Chaban, O.V. Prezhdo, Ab initio molecular dynamics of dimerization and clustering in alkali metal vapors, J. Phys. Chem. A 120 (2016) 4302–4306.
[34] V.V. Chaban, O.V. Prezhdo, Ionic vapor composition in critical and supercritical states of strongly interacting ionic compounds, J. Phys. Chem. B 120 (2016) 4302–4309.